Volume 7 | Number 41 | 7 November 2015 | Pages 17151–17574

Nanoscale

www.rsc.org/nanoscale

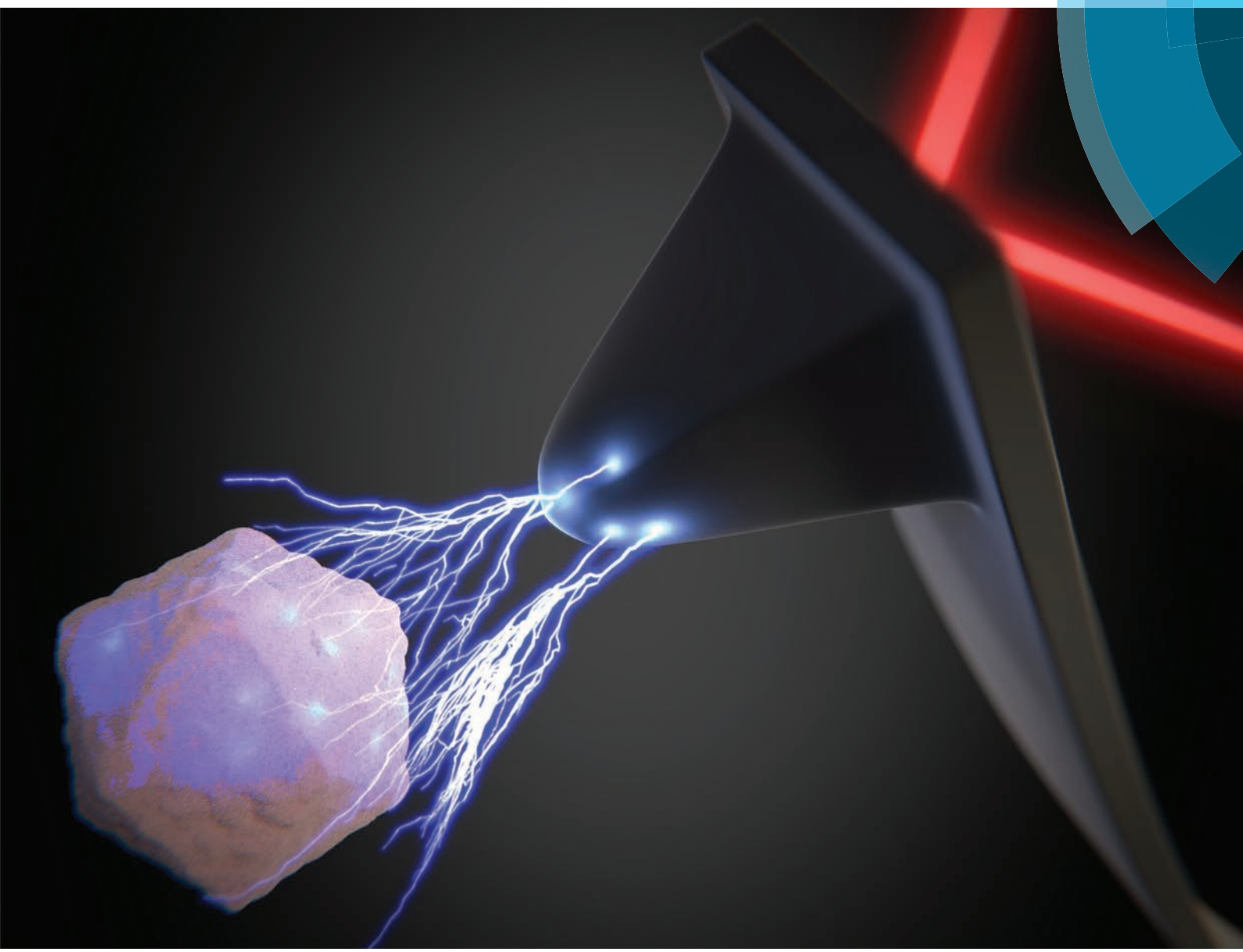

ISSN 2040-3364

ROYAL SOCIETY OF CHEMISTRY

PAPER
R. Podgornik, P. J. de Pablo *et al.*
Quantitative nanoscale electrostatics of viruses

NCNST

Nanoscale

PAPER

View Article Online
View Journal | View Issue

Cite this: *Nanoscale*, 2015, **7**, 17289

Quantitative nanoscale electrostatics of viruses†

M. Hernando-Pérez,‡§[a] A. X. Cartagena-Rivera,¶§[b] A. Lošdorfer Božič,[c,g] P. J. P. Carrillo,[d] C. San Martín,[e] M. G. Mateu,[d] A. Raman,[a] R. Podgornik*[f,g] and P. J. de Pablo*[a]

Received 26th June 2015,
Accepted 16th July 2015

DOI: 10.1039/c5nr04274g

www.rsc.org/nanoscale

Electrostatics is one of the fundamental driving forces of the interaction between biomolecules in solution. In particular, the recognition events between viruses and host cells are dominated by both specific and non-specific interactions and the electric charge of viral particles determines the electrostatic force component of the latter. Here we probe the charge of individual viruses in liquid milieu by measuring the electrostatic force between a viral particle and the Atomic Force Microscope tip. The force spectroscopy data of co-adsorbed ϕ29 bacteriophage proheads and mature virions, adenovirus and minute virus of mice capsids is utilized for obtaining the corresponding density of charge for each virus. The systematic differences of the density of charge between the viral particles are consistent with the theoretical predictions obtained from X-ray structural data. Our results show that the density of charge is a distinguishing characteristic of each virus, depending crucially on the nature of the viral capsid and the presence/absence of the genetic material.

Introduction

The detailed understanding of structural, physical and chemical properties of viruses during their infectious cycle is one of the important challenges facing physical virology.[1] These properties would affect the response of individual viral particles to diverse forces at the nanoscale, which are overwhelmingly present throughout the virus cycle. In particular, nonspecific electrostatic interactions play a central role in different stages of the infectious cycle such as cell entry, maturation, assembly/replication, and exit from the infected cell.[2] It is thus important to quantify the charge of single virus structures in physiological conditions.[3] In this context, traditional techniques used in structural virology, such as cryo-EM or X-ray diffraction, provide high-resolution structural models of virus particles[4] that can be used to infer the corresponding surface charge distribution[5,6] induced by the location of proteins on the capsid and their state of dissociation.[7–10] However, the strong averaging nature of these methods may disguise the effect of viral features not following a symmetrical pattern, such as flexible proteins or disordered genomes. Additionally, using these techniques it is difficult to assess the properties of functional viral particles in physiological conditions.

At the beginning of the 90s, Atomic Force Microscopy (AFM) paved the way for the investigation of electrostatic forces in liquid environments.[11] The subsequent refinement of this technique allowed the measurement of the electrical charge of biomolecules forming monolayers, such as purple membrane[12] resulting in a density of charge of $-0.312e_0$ nm^{-2}, where e_0 is the absolute value of the electron charge (1 C m^{-2} = $6.24e_0$ nm^{-2}). The density of charge of other biomolecules, such as single dsDNA molecules,[13] supported lipid bilayers,[14] and the avidin–streptavidin system[15] have also been measured. In addition, advanced AFM-based dynamic mapping methods have been developed allowing not only the nanoscale resolution of the topography of complex biological systems under physiological conditions, but also relevant physico-chemical properties extracted from the tip–sample interaction.[3,16–18]

[a]*Departamento de Física de la Materia Condensada and Condensed Matter Physics Center - IFIMAC, Universidad Autónoma de Madrid, Spain. E-mail: p.j.depablo@uam.es*
[b]*Birck Nanotechnology Center & School of Mechanical Engineering, Purdue University, IN, USA*
[c]*Max Planck Institute for Biology of Ageing, D-50931 Cologne, Germany*
[d]*Centro de Biología Molecular Severo Ochoa (Consejo Superior de Investigaciones Científicas-Universidad Autónoma de Madrid), Spain*
[e]*Department of Structure of Macromolecules and Nanobiomedicine Initiative, Centro Nacional de Biotecnología/CSIC, Cantoblanco, 28049 Madrid, Spain*
[f]*Department of Physics, University of Ljubljana, SI-1000 Ljubljana, Slovenia*
[g]*Department of Theoretical Physics, Jozef Stefan Institute, SI-1000 Ljubljana, Slovenia. E-mail: podgornik@fmf.uni-lj.si*

†Electronic supplementary information (ESI) available. See DOI: 10.1039/c5nr04274g

‡Present address: Department of Chemistry, Indiana University, Bloomington, IN, USA.
§These authors contributed equally to this work.
¶Present address: Laboratory of Cellular Biology, Section on Auditory Mechanics, National Institute on Deafness and Other Communications Disorders, National Institutes of Health, Bethesda, Maryland, USA.

The study of viruses at a single particle level in liquid milieu with AFM has provided a number of important biophysical discoveries about the interplay between their structure and physical properties.[1,19–22] Force spectroscopy measurements of single viral particles provide not only direct information on their elasticity, but also allow for an estimation of other physical interactions and/or properties, such as rigidity/fragility, viscosity, and adhesion,[18] dielectric properties of constitutive materials,[23] *etc*. Specifically, the quantification and determination of their electrostatic charge in relevant native environments remains unexplored so far.

In buffer conditions and beyond pure mechanics, there is a plethora of long and short-range forces that affect the interaction between an AFM tip and a virus particle.[24] In the most commonly used theoretical framework of the Derjaguin–Landau–Verwey–Overbeek (DLVO) theory, they are *grosso modo* differentiated into the usually attractive van der Waals (vdW) and repulsive electrostatic double layer (EDL) forces.[25] Other interactions such as solvation forces of the hydrophobic and hydration types, or entropic forces such as the Helfrich interaction or polymer-mediated forces, are usually considered to be much more specific, depending on the details of the interacting materials as well as the intervening solvent.[26] While being simplistic in nature, the DLVO framework allows for a quantitative interpretation of the measured force data and indeed provides a guideline for their characterization and manipulation. Most notably, it accounts for the interpretation of the range of the EDL interactions *via* the Debye screening length and for the strength of the vdW interactions *via* the Hamaker coefficients. Other properties of the solution, such as the nature of the solvent[27] and/or the pH, are less straightforward to incorporate into the DLVO framework.[28] Nevertheless, the DLVO theory has been successfully applied also in the context of interactions between biological materials providing for at least some rationalization of the observed interactions between lipid membranes[29] or individual molecules of DNA.[30] It seems only natural to expect that these interactions govern also the forces between the probe tip, the substrate and any sample under investigation in the AFM force spectroscopy.[13,18,31]

In this work we utilize force spectroscopy to characterize the electrostatic interactions between the AFM tip and different kinds of virus particles that are simultaneously adsorbed on the same substrate. By using the DLVO theory, we have extracted the charge density of ϕ29 prohead and virion, adenovirus, and the capsid of minute virus of mice (MVM) in physiological conditions and identified their determinants to be the virus shell intrinsic structure and the absence/presence of viral genome inside.

Results

Electrostatics of viral particles in solution

Electro-mechanical characterization of individual viral capsids adsorbed on HOPG (Highly Oriented Pyrolytic Graphite) has been performed with force spectroscopy assays using the AFM.[13] The monovalent salt concentration of the solution, [salt] in units of moles per liter, sets the Debye length as $\lambda_D = \frac{0.304}{[\text{Salt}]^{\frac{1}{2}}}$ in nm. For a typical concentration of 2 mM NaCl salt, we have $\lambda_D \sim 6.8$ nm.[32] Fig. 1 shows a collection of force *vs.* *Z* piezo displacement curves (*F*–*Z*) performed along a line-scan using Force–Volume AFM mode,[33] that accounts for the HOPG substrate (#1, #2, #6, and #7) and a bacteriophage ϕ29 viral particle (#3, #4, and #5) in solution at 2 mM NaCl concentration and pH = 7.8. When the AFM probe approaches close to a virus particle, a repulsive electrostatic interaction is clearly detected a few nanometers away from the surface of the viral particle. In contrast, the absence of surface charge of HOPG allows the vdW force to induce the jump-to-contact of the tip to the substrate.[25]

To compensate for the contribution of virus deformability, short range vdW and hydration forces that may hinder the electrostatic interaction, *F*–*Z* curves need to be rescaled when the AFM probe tip approaches closer than ~2 nm. Fig. 2a presents the fundamentals of the tip–sample interaction and

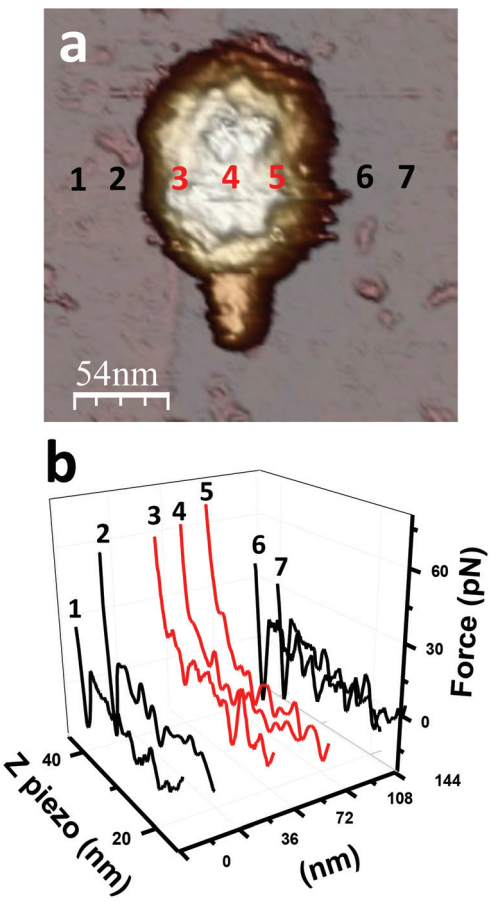

Fig. 1 The electrostatic force of a virus. (a) AFM topography image of a bacteriophage ϕ29 mature virion absorbed on a HOPG surface. (b) *F*–*Z* selected curves performed in a scan line using Force Volume AFM mode on HOPG (#1, 2, 6, and 7, black line) and ϕ29 virion (#3, 4, and 5, red line).

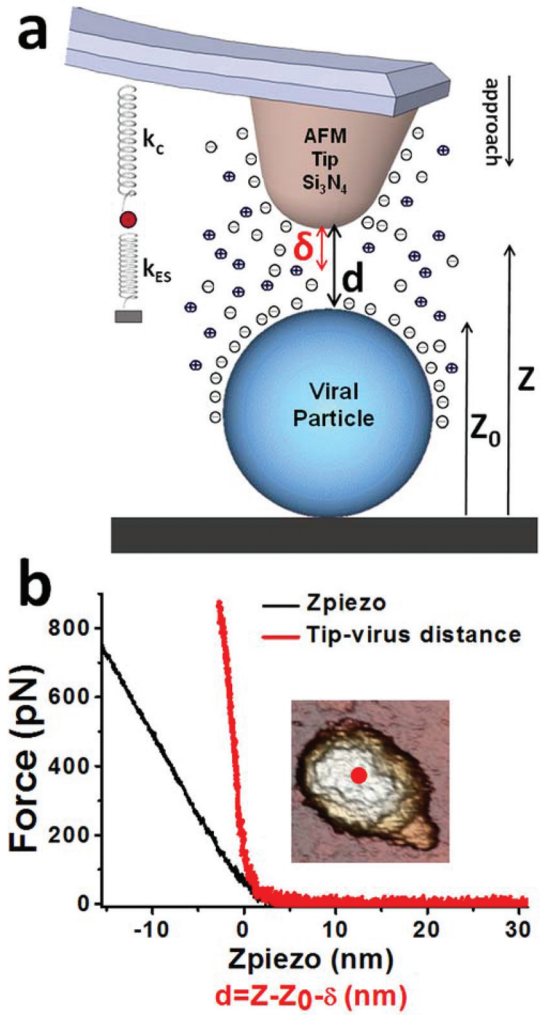

Fig. 2 Basis of electrostatics with AFM. (a) Schematic representation of a single force spectroscopy assay on a viral particle under low salt concentration buffer. Z is the piezo displacement, Z_0 is the point of contact, δ is the deflection of the cantilever, k_c is the spring constant of the cantilever, k_{ES} is the effective spring due to electrostatic and vdW forces and $d = Z - Z_0 - \delta$ is the effective tip–virus gap since viral deformation is negligible for repulsive forces under 100 pN. (b) A comparison between F–Z and F–d curves performed on viral particle.

sample force spectroscopy in an AFM F–Z curve under low salt concentration conditions. On close approach of the AFM probe tip to the viral particle, the large repulsive force induces a deflection of the cantilever, and thus the F–Z curve needs to be properly corrected to obtain the real probe tip–virus distance, as presented in Fig. 2b. This correction is achieved by using the standard AFM force spectroscopy methods for deformable surfaces[18,34] and yields the effective gap distance $d = Z - Z_0 - \delta$, where Z is the piezo displacement, Z_0 is the point of contact and δ is the perpendicular deflection of the cantilever (ESI Fig. S1†). Note that viral deformation is negligible as long as the forces are smaller than 100 pN (Fig. S1d†). AFM is a technique prone to various artifacts affecting force spectroscopy. In particular, the electrostatic force strongly depends on the total charge of the tip and its eventual contamination. Since the tip conditions affecting its charge may vary from tip to tip, it is important to perform the experiments with the same tip in different specimens. One option to fulfill this condition is to co-adsorb all the different viral specimens in the same substrate for utilizing the same tip. Fig. 3a shows the simultaneous adsorption of different types of viral particles on a HOPG surface. We measured F–Z curves on different populations of viral particles, consisting of 12 ϕ29 virions, 7 ϕ29 proheads, 8 adenovirus, and 11 MVMs (Fig. 3a) over 12 independent experiment sets. We converted F–Z into force *vs.* tip–virus gap distance (F–d) curves by systematically accounting for cantilever deflection, as shown in Fig. 2b. Since the surface of mica presents a charge density of -0.0025 C m^{-2} or $0.015e_0$ nm^{-2},[32,35] it is crucial to use its value for finding the expected λ_D. In our case, using 2 mM NaCl salt concentration, we adjust λ_D to be 6.8 nm. Fig. 3b shows an example of a F–d curve obtained on the mica surface that yields an excellent fit to the screened electrostatic repulsion, with no indication of either attractive vdW forces or repulsive solvent mediated forces in the separation regime of 3.5–20 nm, as expected.[36] Thus, for testing purposes, it is encouraging to find experimentally a similar $\lambda_D \sim 6.8$ nm from the fitting of the force spectroscopy on the mica surface to the generic DLVO interaction.[32] In fact this verification allows us to determine whether the AFM-tip is contaminated, since any attached debris would affect its size and density of charge.

The acquired and rescaled F–d curves obtained for viral particles were individually fitted using an *Ansatz* expression based of the double exponential Parsegian–Gingell model[37,38] and its implementation to curved surfaces. This implementation quantifies the electrostatic interaction between two curved, dissimilarly charged surfaces in the whole range of minimal separation distances, d, between the interacting surfaces (Materials and methods, M&M). The model parameters A and B, containing information about the surface charge densities of the tip and the sample, were extracted by fitting the F–d curve on a viral particle at a predetermined value of the inverse Debye screening length $\kappa = \frac{1}{\lambda_D}$ and distance d (M&M).

$$F(d) = (Ae^{-2\kappa d} + Be^{-\kappa d})/(1 - e^{-2\kappa d}). \quad (1)$$

Fig. 3c shows typical curves for ϕ29 virion, ϕ29 prohead, adenovirus and MVM capsid. From a total of 87 F–d curves obtained for ϕ29 virions (30), ϕ29 proheads (12), adenoviruses (24), and MVM particles (21), we extracted the electrostatic interaction force between the tip and the surface of each type of virus and for different values of λ_D, (Table 1). Fig. S2† shows data of the interaction force coefficient B (*Mean* ± *Standard Deviation*) which contains information from different co-adsorption experiments at 6.8 nm Debye length. The results of fitting show that the B coefficient is on the order of ~10 pN, *i.e.*, 25 ± 8 pN, 16 ± 5 pN, 20 ± 7 pN and 4 ± 2 pN for ϕ29 virion, ϕ29 prohead, adenovirus, and MVM capsid, respectively. Because of higher screening the contribution of coeffi-

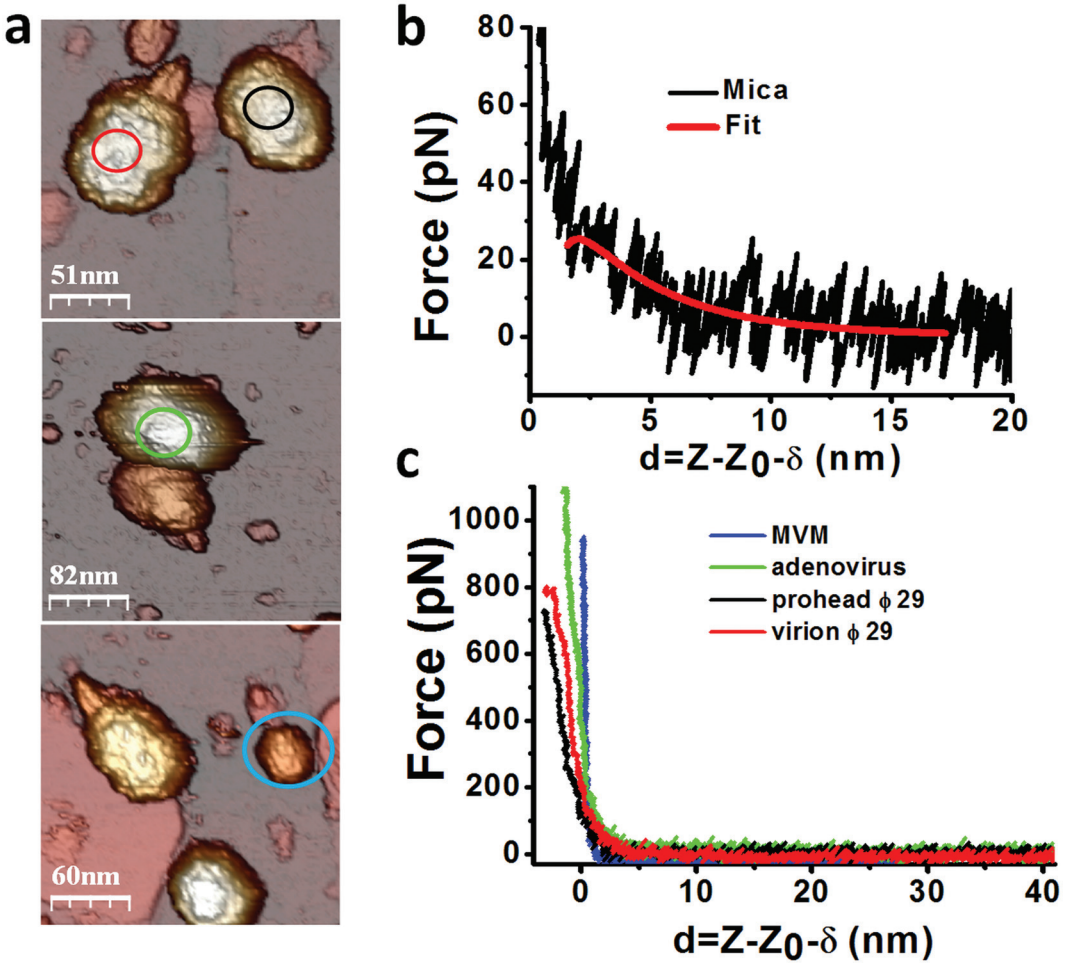

Fig. 3 Co-adsortion of viruses. (a) AFM topography images of co-adsorbed of viral particles: ϕ29 virion (red circle), ϕ29 prohead (black circle), adenovirus (green circle), and MVM capsid (blue circle). (b) *F–d* curve performed on mica in 2 mM NaCl salt concentration buffer. The mica data plot has been fitted using a generic DLVO approximation (red line) and clearly shows the good agreement of the fit. (c) *F–d* curves collected on the viral particles ϕ29 virion (red), ϕ29 prohead (black), adenovirus (green), and MVM (blue).

Table 1 Summary of quantitative electrostatic data (*B* and surface charge density as (*Mean* ± *Standard Deviation*)) from the fitting of multiple *F–d* curves obtained for viral particles using eqn (2) under two different salt concentration buffers. 87 *F–d* curves were obtained for 38 viral particles (12 particles of ϕ29 virions, 7 particles of ϕ29 proheads, 8 particles of adenovirus and 11 MVM) at 2 mM NaCl pH = 7.8, λ_D = 6.8 nm; and 32 *F–d* curves performed on 16 viral particles (10 particles of ϕ29 virion and 6 particles of ϕ29 prohead) at 10 mM NaCl pH = 7.8, λ_D = 3 nm

	Virion ϕ29		Prohead ϕ29			
Parameters	λ_D = 6.8 nm, d > 1 nm	λ_D = 3 nm, d > 1 nm	λ_D = 6.8 nm, d > 1 nm	λ_D = 3 nm, d > 1 nm	Adenovirus λ_D = 6.8 nm, d > 1 nm	MVM λ_D = 6.8 nm, d > 1 nm
B (pN)	25 ± 8	60 ± 27	16 ± 5	47 ± 13	20 ± 7	4 ± 2
Sigma (C m^{-2})	−0.0114 ± 0.0035	−0.06 ± 0.03	−0.0074 ± 0.0020	−0.05 ± 0.01	−0.0085 ± 0.0020	−0.0023 ± 0.0014
#Particles	12	10	7	6	8	11
#*F–d* curves	30	20	12	12	24	21

cient *A* was found to be negligible in comparison with coefficient *B*. After fitting and extracting the numerical values of the coefficients, we proceeded to estimate the surface charge density of different viral particles according to the Parsegian–Gingell model, obtaining statistically significant differences between the viruses.

Fig. 4 shows the values for surface charge density (*Mean* ± *Standard Deviation*) which contains information from different co-adsorption experiments at $\lambda_D \sim 6.8$ nm. The estimated values for surface charge density are: −0.0114 ± 0.0035 C m^{-2} (−0.071 ± 0.022e_0 nm^{-2}), −0.0074 ± 0.0020 C m^{-2} (−0.046 ± 0.012e_0 nm^{-2}), −0.0085 ± 0.0020 C m^{-2} (−0.053 ± 0.012e_0

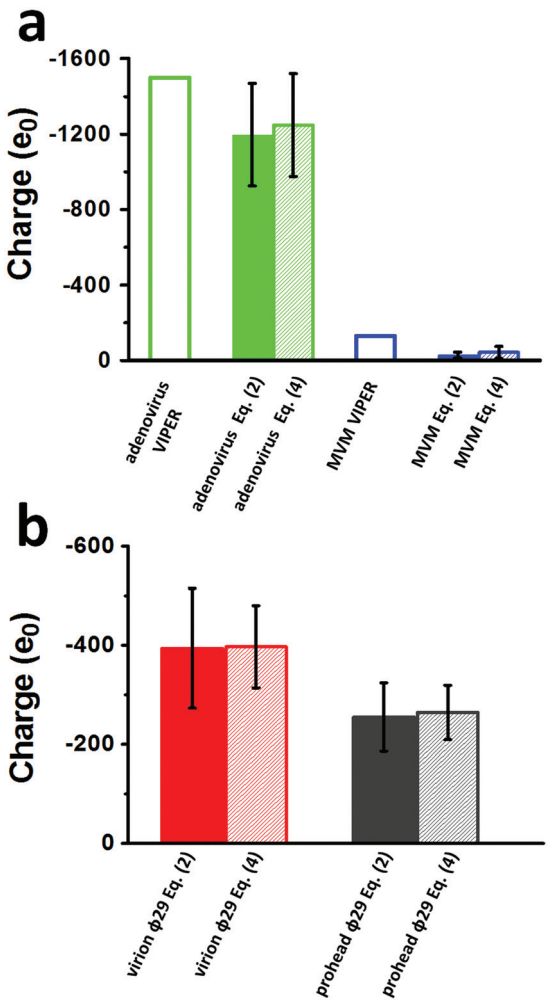

Fig. 4 Viral particle identification by quantifying the total fitted charge. (a) Comparison between viral particle charge estimated from VIPERdb (empty columns) as described in Fig. 5 and extracted from experimental data analysis using eqn (2) (solid columns) and eqn (4) (sparse columns) respectively (*Mean ± Standard Deviation*) of the viral particles under 2 mM NaCl with pH = 7.8 buffer conditions: 8 particles of adenovirus (green bar) and 11 particles of MVM (blue bar). (b) Charge of bacteriophage ϕ29: 12 virions (red bar) and 7 proheads (black bar) extracted from experimental data analysis using eqn (2) (solid columns) and eqn (4) (sparse columns). For the VIPERdb estimate we use the approximate average of the full charge obtained from Fig. 5.

nm^{-2}), and -0.0023 ± 0.0014 C m^{-2} ($-0.014 \pm 0.008 e_0$ nm^{-2}) for ϕ29 virion, ϕ29 prohead, adenovirus, and MVM capsid, respectively (Table 1). Thus, we can estimate the total charge by considering viruses as spheres. These would correspond to charges of $Q_{\phi 29} = -394 \pm 121 e_0$, $Q_{\text{prohead}\phi 29} = -255 \pm 69 e_0$, $Q_{\text{adenovirus}} = -1197 \pm 272 e_0$, and $Q_{\text{MVM}} = -28 \pm 16 e_0$ (ESI Table S1†). Furthermore, one-way ANOVA analysis of these results shows that the ϕ29 virion and the ϕ29 prohead display significant statistical differences ($P < 0.035$), while there is none between the ϕ29 virion and the adenovirus ($P > 0.05$). The force magnitude and the characteristics of electrostatic interactions can be effectively controlled by changing the salt concentration and the pH of the buffer solution.[12] Therefore, we also performed an experimental control at different salt concentration ($\lambda_D \sim 3$ nm) to validate the Parsergian–Gingell model (Fig. S3†).

Discussion

A virus particle portrays a certain distribution of charge due to the particular organization of proteins within its structure, which is a fingerprint of each type of virus. Therefore, the validation of our methodology requires systems where it is possible to estimate the charge independently.[6] In particular, the charge of MVM and adenovirus shells can be estimated from the VIPERdb[5] and thus, they are excellent candidates for an experimental validation. The VIPERdb contains the full (3D) spatial charge distribution of adenovirus 5 (entry IDs 3iyn) and MVM (entry, ID 1z14) (for details see ref. 6). Inner (Q_{in}) and outer (Q_{out}) charge on the capsids were obtained from the VIPERdb at neutral pH, including only aminoacids inside the inner (outside the outer) surface of the virus as described in detail in ref. 6. Since these surfaces and therefore their corresponding radii R_{in} and R_{out} are not unequivocally defined, different values can be obtained also for Q_{in} and Q_{out}, as well as for the full structural charge equal to the sum $Q_{in} + Q_{out}$, when the exact position of these two surfaces is varied. When comparing with experimentally obtained values in Fig. 4, we therefore list an average that we estimate from different positions of R_{in} (R_{out}) as shown in Fig. 5. For adenovirus the average of the full structural charge is then $Q_{in} + Q_{out} \sim -1500 e_0$, and for MVM $Q_{in} + Q_{out} \sim -130 e_0$. We should also state here that it is not clear at this point which part of the inner charge, if at all, the AFM electrostatic force spectroscopy is sensitive to and the comparison with experimentally obtained values should be evaluated in this light.

A comparison of the structural virus charge of different virus types with the values extracted from experiments, in particular for adenovirus, in general supports our experimental approach (Fig. 4a and ESI Table S1†). The measured charge of MVM particles presents the lowest value and the highest Standard Deviation (SD). Interestingly, the estimation of the charge of MVM from VIPERdb also points to the lowest charge, which is ~10 times less than the adenovirus one in both cases. Correspondingly, MVM capsid presents the lowest tip–sample electrostatic interaction force ($B \sim 4$ pN). In cases of low charge, the determination of its value is likely affected by the thermal noise of the cantilever. The thermal noise introduces an intrinsic limitation to the measurement of the force out of contact. Specifically, the signal of the deflection shows a thermal noise of about 10 mV for RC800PSA-Olympus microcantilevers, (spring constant 0.05 N m^{-1}), with a bending-optical calibration of 20 nm V^{-1}. Thus, the thermal noise introduces an uncertainty in the measured force of 0.05 (N m^{-1}) × 20 (nm V^{-1}) × 0.01 V ~ 10 pN. Therefore, the Brownian motion of the cantilever restricts the measurement of forces below 10 pN. Since the interaction force between MVM and the tip is ~4 pN (Table 1),

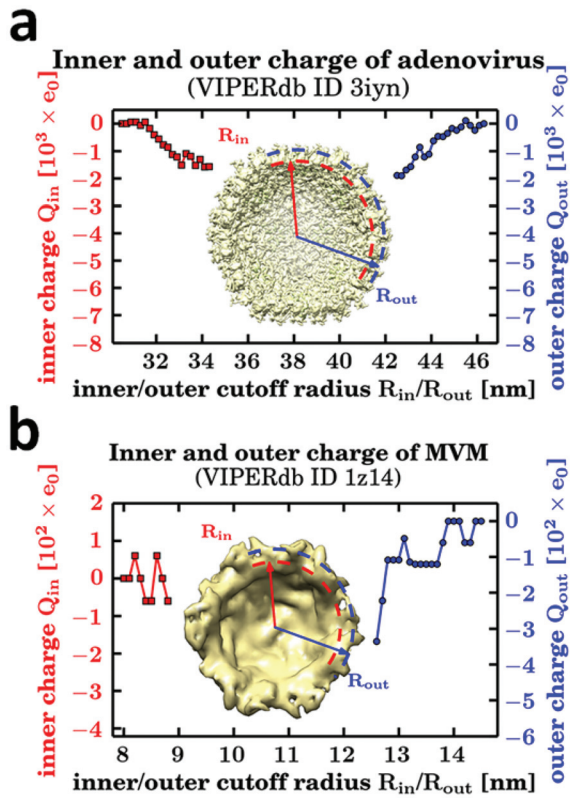

Fig. 5 Structural charge of the capsid estimated from VIPERdb. Inner (Q_{in}) and outer (Q_{out}) charge of adenovirus (a) and capsids of MVM (b) obtained from the VIPERdb as described in ref. 6. The charge was calculated at neutral pH, including only aminoacids inside the inner (outside the outer) surface of the virus. As these surfaces are not unequivocally defined their corresponding radii R_{in} and R_{out} are varied leading to different values of inner (red) and outer (blue) total charge. The full charge of the structural charge would then be the sum of the two. The inner and outer surface radius was varied from their values at the full-width half-maxima (FWHM) of the mass density distributions of the capsids: R_{in} = 34.3 nm, R_{out} = 42.4 nm for adenovirus and R_{in} = 7.79 nm, R_{out} = 12.5 nm for MVM. The insets show the capsids with drawn positions of the varied inner and outer surfaces. Half-capsids shown in insets were drawn with UCSF Chimera.[55]

the detection of the electrostatics of MVM is below our sensitivity, resulting in a high SD. Still, the experimental result for MVM point to a very low charge value, in complete agreement with the calculated value from the MVM VIPERdb data.

Once our methodology was validated, we interrogated the influence of the genome on the charge density of the virus particle. To this effect we chose both ϕ29 prohead and virion since, except for the tail, their respective shell are comprised of identical proteins.[39] Thus, it is possible to isolate the electrostatic effect of the 19.8 kbp of dsDNA packed inside.[40] Our results show that the virion presents a charge density ~30% larger than the prohead (Fig. 4b). Thus, the genome has a significant effect on the overall electrostatic interaction forces due to the large amount of associated negative charge of the deprotonated phosphates.[41]

Interestingly, this is not the case in adenovirus particles. Although the density of charge obtained from our experiments corresponds to DNA-full particles, they show a reasonable agreement with the VIPER data, which accounts only for the charges of the adenovirus shell. This absence of influence of the adenovirus genome on the measured electrostatic charge might be related with the DNA condensation mechanism. Contrariwise to bacteriophage ϕ29, the encapsidated dsDNA in adenovirus is condensed by histone-like proteins that carry a large net positive charge,[42] which might partly compensate the DNA charge nearly neutralizing it.

To check the robustness of our measurements we performed control experiments in buffer at higher salt concentration ($\lambda_D \sim 3$ nm). The viral particles of bacteriophage ϕ29 present different values of interaction force coefficient B when the Debye length was changed (Fig. S3†), but the ratio of the coefficient B for different salts remains constant at ~1.3 for both salt concentration buffers and for the ϕ29 virion and the prohead (Table 1). Therefore, changes in Debye length do not significantly modify the estimated value of the electrostatic charge in individual viral particles. This is consistent also with experiments on purple membrane adsorbed to alumina in electrolyte solutions, pointing to a general feature of the DLVO interactions at large enough separations.[12]

The comparison between the structurally estimated charge and the experimentally extracted values follows a reasonable trend, even with low confidence value as is the case for weakly charged MVM. In our opinion the latter adds firm support to the general experimental methodology for the analysis for electrostatic force spectroscopy on complex mesoscopic aggregates of nucleoproteins. In this respect, our experiments pave the way to a more general force spectroscopy of any either natural or artificial protein cages with synthetic cargos, set quite apart from mechanical elasticity probing, allowing us to interrogate a different set of parameters that convey essential information on the nature and magnitude of interactions acting on this scale in Nature.

Materials and methods

AFM experiments

To properly quantify the electrostatic force spectroscopy data, we first identified and imaged viral nanoparticles in buffer solution by operating in the Jumping Plus Mode (Nanotec Electrónica S.L., Madrid, Spain),[43] while using rectangular silicon nitride RC800PSA (Olympus, Tokyo, Japan) cantilevers with nominal spring constants of ~0.05 N m^{-1}, and nominal tip radius of ~15 nm. The maximum force applied during each scan never exceeded 100 pN with a velocity of 0.3 lines per second to prevent the damage of the viral shells. The optical photodetector cantilever sensitivity was obtained by recording a force *vs.* Z piezo displacement curve (F–Z) on a stiff substrate. Cantilever effective spring constants were routinely calibrated using the Sader's method.[44]

After recording an image with multiple viral particles, we gently deformed each individual capsid by performing five *F–Z* curve measurements on the top of the viral particles: the shell is zoomed-in continuously by reducing the *x–y* scanning size until the bump of the very top is within the whole piezo scan. Until ~400 pN the viral particles show a linear elastic deformation[34] which provides the spring constant of the virus k_v (modeled as a spring in series with the cantilever). Following each *F–Z* curve-set, an image of 128 × 128 points of the viral particle is recorded to monitor its integrity, as well as to know its position in order to correct for any drift if needed for the next *F–Z*s set. The *F–Z*s speed was ~60 nm s^{-1}. Images were post-processed using the WSxM software.[45]

Data analysis

To study the electrostatic interactions between the probe tip and the viral particle, we need to define the interaction model that best describes the behavior of the force at a tip–sample gap within the measured range of 1–20 nm. This range is just outside the complicated short-range interaction regime (~1 nm before contact),[27] so that we can neglect the effects of hydration and/or vdW interactions that are present in that regime.[25] Eliminating in this way all but electrostatic interactions in the regime of experimentally accessible separations that certainly simplifies the problem, leaving us with the question of the most appropriate form of these interactions. Since our system is fundamentally asymmetric, with heterogeneous probe–tip and virus particle surfaces, having in general quite distinct charge properties, we assume that the electrostatic interactions are properly described by two dissimilarly charged surfaces. Furthermore, the surface charges are surmised to be constant, *i.e.* they do not vary as the two interacting surfaces are brought closer together, which is the essential assumption of the Parsegian–Gingell model. While this is certainly true for the AFM tip, for the proteinaceous shell charge regulation[46] would be a better assumption. However, recent implementation of the charge regulation model for viral shells[28] makes the assumed constancy of surface charge a reasonable approximation to work with.

For small separations compared with the curvature radii, the electrostatic force, F_{ts}, between the tip and the substrate of respective curvatures $(R_t)^{-1}$ and $(R_s)^{-1}$, can then be obtained *via* the standard Derjaguin approximation[25] that connects it with the interaction free energy between two flat surfaces $W(d)$ as:

$$F_{ts}(d) = 2\pi R_{eff} W(d), \quad (2)$$

where R_{eff} is the effective radius of curvature given by $(R_{eff})^{-1} = (R_t)^{-1} + (R_s)^{-1}$ and $W(d)$ is the surface interaction free energy density given by the Parsegian–Gingell expression:[37]

$$W(d) = (1/\varepsilon\varepsilon_0\kappa)[(\sigma_\tau{}^2 + \sigma_s{}^2)e^{-2\kappa d} + 2\sigma_\tau\sigma_s e^{-\kappa d}]/(1 - e^{-2\kappa d}), \quad (3)$$

where ε and ε_0 are the dielectric constant of water and vacuum permittivity, σ_τ, σ_s are the surface charge densities of the tip and the substrate, and κ is the inverse Debye screening length $\kappa = 1/\lambda_D = 0.304$ nm/[I], for a monovalent salt solution where I is the ionic strength in M/l [25]in accordance with the interaction models used previously.[12,32]

For fitting purposes, we then worked with the *Ansatz* expression of a double exponential $F_{ts}(d) = (Ae^{-2\kappa d} + Be^{-\kappa d})/(1 - e^{-2\kappa d})$ in the interval of the tip-substrate separation $d \sim$ 1–20 nm. The constraint connecting both fitting coefficients A and B is evident from comparison with eqn (2). The actual range for the fit was chosen so that it yields the best-adjusted R-square values (see Fig. S4†). To estimate the A and B fitting coefficients we assumed the following values of the specific parameters: surface charge density of the tip $\sigma_t = -0.0025$ C m^{-2},[47] radius of the tip $R_t = 15$ nm, and radius of the virus particle $R_s = 21.5$ nm, 47.5 nm, and 12.5 nm for the ϕ29, adenovirus and MVM particles, respectively.[9,10,19,38]

For separations much larger compared with the curvature radii, the distance decay of the Derjaguin expression eqn (3), *i.e.* a screened exponential form $\exp(-\kappa d)$, is inconsistent with the faster (and correct) decay of a screened Coulomb potential between two point-like charges, which is $\exp(-\kappa R)/R$, where $R = d + R_t + R_s$. This is due to the fact that in this limit the effect of surface curvature becomes non-perturbative and can not be described by the Derjaguin approximation anymore.[48] As a consequence the interaction free energy and the interaction force decay faster with separation than for two planes. While not as straightforward as the Derjaguin approximation, an excellent approximation can nevertheless be obtained also in this case by variety of methods.[49,50] Based on the two approximate forms valid for small and large separations, it is then possible to construct an interpolation formula that is valid in both regimes of small as well as large separations, and consists of simply replacing R_{eff} in eqn (2) by:

$$R_{eff} = R_tR_s/(R_t + R_s) \rightarrow R_tR_s/(d + R_t + R_s) = R_tR_s/R,$$

giving the interaction force as:

$$F_{ts}(d) = (2\pi R_tR_s/\varepsilon\varepsilon_0\kappa R)[(\sigma_\tau{}^2 + \sigma_s{}^2)e^{-2\kappa(R-R_t-R_s)} + 2\sigma_\tau\sigma_s e^{-\kappa(R-R_t-R_s)}]/(1 - e^{-2\kappa(R-R_t-R_s)}), \quad (4)$$

where $R = d + R_t + R_s$. Note that for large separations this is not equivalent to the Derjaguin approximation, though it looks very similar to it, as it decays like a screened Coulomb interaction potential between two point particles, *i.e.* as $\exp(-\kappa d)/R$.[48] As a side note, the interpolation formula also corrects for an overestimation inherent in the Derjaguin approximation.

The interpolation formula now shows the correct behavior at small separation, where it approaches the screened electrostatics interaction free energy between two planar surfaces, as well as at large separations where it approaches the screened electrostatic interaction free energy between two point-like charges. While being consistent in their respective limiting behaviors, numerically and for the range of separations relevant here, the expressions eqn (2) and (4) are practically indistinguishable, see Fig. 4, ESI Tables S1 and S2.†

F–d fitting protocol

To successfully fit the electrostatic interaction model to the response curve we generated a MATLAB code. First, the experimental curves were smoothed by using a Gaussian moving average filter on the raw response data. After smoothing, we use the nonlinear least squares method to best fit the filtered data and extract the parameters of interest. Because we want to have a rigorous way to analyze the data we use goodness of fit statistical method to calculate the R^2 value and an estimate of the error variance. We pursued for the best R^2 value (see Fig. S4†). From this procedure we can estimate the coefficients A and B of the electrostatic interaction force, when the decay length λ_D is fixed (6.8 nm), starting at a distance $d \sim 1$ nm and ending at ~20 nm. Since coefficient A is much more screened then B, see eqn (2) and/or (4), we have excluded it from further consideration. From the fitted B value we finally estimate the density of charge of the viral shell.

Viruses description

ϕ29 prohead and mature virion. The bacteriophage ϕ29 shell is assembled by the interaction of the connector protein (gp10), the scaffolding protein (gp7) and the major head protein (gp8). The connector is a dodecameric assembly which is located in one of the 12 five-fold vertices.[51,52] The correct interaction of the connector, the scaffolding protein and the major protein is required for the generation of the characteristic prolate icosahedra (54 nm × 42 nm). The shell of the ϕ29 bacteriophage contains 235 gp8 subunits arranged with a T = 3, Q = 5 lattice with 11 pentameric plus 20 hexameric units forming icosahedral end caps, and 10 hexameric units forming the cylindrical equatorial region.[9,53] An additional component of the shell are fibers (made of protein gp8.5), which are indispensable for virus infectivity. For the mature virion, DNA packaging is accompanied by the release of the scaffolding protein.[40] After completion of the DNA encapsidation, the connector interacts with the other tail components (gp11, gp12 and gp9) to secure the placement of DNA inside the head shell and the positioning of the tail components in a unique five-fold vertex of the capsid. The ds-DNA molecule of 19.8 kbp (6.3 μm long) is densely packed inside the viral particle at almost close packing conditions.

Human adenovirus

The human adenovirus genome is a linear dsDNA molecule of approximately 35 kbp. Positively charged proteins of viral origin help to condense the DNA so that it fits within an icosahedral protein shell of approximately 95 nm vertex-to-vertex diameter. Most of the shell is composed by the major coat protein (hexon), except for the vertices of the icosahedron, which are occupied by a complex formed by the penton base and fiber proteins. The penton base, and particularly the fiber, are critical in the infectious process, because they regulate the binding to specific virus receptors in the cell membrane and trigger the process of cell entry. Adenovirus requires at least four other proteins (called "minor" or "cementing" proteins) to successfully assemble a stable shell that will safely carry the viral genome to a new host cell for proliferation of the virus.[10] Adenovirus samples used in this work were purified as described in.[54]

Minute virus of mice (MVM)

The parvovirus minute virus of mice (MVM) is among the smallest and structurally simplest viruses known. The parvovirus capsid is formed by 60 structurally equivalent subunits arranged in a simple (T = 1) icosahedral symmetry and approximately 25 nm in diameter. The capsids used are formed by 60 identical copies of capsid protein VP2, and are devoid of the viral single-stranded DNA contained in the virion.

AFM sample preparation

ϕ29 prohead and virion stocks of viral particles were stored in TMS buffer (10 mM $MgCl_2$, 50 mM Tris and 100 mM NaCl, pH 7.8). Adenovirus stocks of particles were stored in HBS buffer (20 mM Hepes and 150 mM NaCl, pH 7.8). MVM capsids stocks of particles were stored in PBS buffer (phosphate-buffered saline pH 7.4 containing 150 mM NaCl). A drop of 20 μl stock solution of all viral particles was deposited and left on a freshly cleaved HOPG (ZYA quality NTMDT), for about 30 min. Then, the sample was rinsed 6 times with different concentration of NaCl solution to progressively reach the final electrolyte concentration condition of 2 mM NaCl (10 mM, 5 mM, and 2 mM, respectively). Samples were left to stabilize for 5 min after each solution change to prevent osmotic shock. In parallel we rinsed freshly cleaved mica in the same way in order to detect the control Debye length resulting at the final NaCl concentration. In this way *F–Z* curves were acquired on freshly cleaved mica to obtain the experimental Debye length at this condition as described in the main text. In the presence of electrolyte solutions, charged surfaces develop an electrical double layer interaction whose decay length depends on the ion concentration of the solution (eqn (3)).[25] The theoretical value of λ_D is 6.4 nm and the experimental value obtained by fitting the *F–d* curve acquired on the mica was ~6.8 nm, which indicates an error < 10%.

Conclusions

We have explored and determined the electrostatic charge of different viral particles in buffer solutions using single force–distance assays in a nanoscale electrostatic force spectroscopy. The presented findings indicate statistically significant, measurable differences in the electrostatic charge between different virus types, and thus pave the way for electrostatic identification of viruses and nanoparticles in aqueous solutions by probing only the long-range electrostatic interactions with an AFM tip. We conclude that the electrostatic interaction force between the charged AFM tip and the virus capsid depends crucially on the nature of the viral capsid and the presence of packed genetic material. We propose that electro-

static force spectroscopy could be well suited for non-invasive probing and identification of virus capsids and their molecular cargo.

Acknowledgements

We acknowledge Prof. V. Adrian Parsegian for insightful discussion. PJP acknowledges MINECO of Spain through project FIS2011-29493, FIS2014-59562-R, and the Spanish Interdisciplinary Network on the Biophysics of Viruses (Biofivinet, FIS2011-16090-E). CSM acknowledges funding from BFU2013-41249-P, and Biofivinet. MGM acknowledges funding from the Spanish Government (BIO2012-37649), Comunidad de Madrid (S-505/MAT-0303), and by an institutional grant from Fundación Areces to the Centro de Biología Molecular. RP acknowledges support from Slovenian Agency for Research and Development (ARRS) grant Nos. P1-0055, J1-4297, and J1-4134. AR acknowledges funding from the National Science Foundation Materials Network grant DMR 1008189 "Probing *in vitro* Structure–Property–Function Relationships of Viruses at High-Resolution using Advanced Atomic Force Microscopy Methods". PJP and RP acknowledge the Aspen Center for Physics and NSF grant # 1066293.

Notes and references

1 W. H. Roos, R. Bruinsma and G. J. L. Wuite, *Nat. Phys.*, 2010, **6**, 733–743.
2 A. Siber, A. L. Bozic and R. Podgornik, *Phys. Chem. Chem. Phys.*, 2012, **14**, 3746–3765.
3 S. Zhang, H. Aslan, F. Besenbacher and M. D. Dong, *Chem. Soc. Rev.*, 2014, **43**, 7412–7429.
4 J. R. Caston, in *Structure and Physics of Viruses*, ed. M. G. Mateu, Springer, The Netherlands, 2013, vol. 68, ch. 3, pp. 79–115.
5 M. Carrillo-Tripp, C. M. Shepherd, I. A. Borelli, S. Venkataraman, G. Lander, P. Natarajan, J. E. Johnson, C. L. Brooks and V. S. Reddy, *Nucleic Acids Res.*, 2009, **37**, D436–D442.
6 A. L. Bozic, A. Siber and R. Podgornik, *J. Biol. Phys.*, 2012, **38**, 657–671.
7 I. K. Robinson and S. C. Harrison, *Nature*, 1982, **297**, 563–568.
8 J. Tang, N. Olson, P. J. Jardine, S. Girimes, D. L. Anderson and T. S. Baker, *Structure*, 2008, **16**, 935–943.
9 Y. Z. Tao, N. H. Olson, W. Xu, D. L. Anderson, M. G. Rossmann and T. S. Baker, *Cell*, 1998, **95**, 431–437.
10 C. San Martín, *Viruses*, 2012, **4**, 847–877.
11 H. J. Butt, *Biophys. J.*, 1991, **60**, 1438–1444.
12 H.-J. Butt, *Biophys. J.*, 1992, **63**, 578–582.
13 J. Sotres and A. M. Baro, *Biophys. J.*, 2010, **98**, 1995–2004.
14 G. Gramse, A. Dols-Perez, M. A. Edwards, L. Fumagalli and G. Gomila, *Biophys. J.*, 2013, **104**, 1257–1262.
15 L. Almonte, E. Lopez-Elvira and A. M. Baró, *ChemPhysChem*, 2014, **15**, 2768–2773.
16 M. D. Dong, S. Husale and O. Sahin, *Nat. Nanotechnol.*, 2009, **4**, 514–517.
17 A. Raman, S. Trigueros, A. Cartagena, A. P. Z. Stevenson, M. Susilo, E. Nauman and S. A. Contera, *Nat. Nanotechnol.*, 2011, **6**, 809–814.
18 A. Cartagena, M. Hernando-Pérez, J. L. Carrascosa, P. J. de Pablo and A. Raman, *Nanoscale*, 2013, **5**, 4729–4736.
19 C. Carrasco, A. Carreira, I. A. T. Schaap, P. A. Serena, J. Gomez-Herrero, M. G. Mateu and P. J. Pablo, *Proc. Natl. Acad. Sci. U. S. A.*, 2006, **103**, 13706–13711.
20 C. Carrasco, A. Luque, M. Hernando-Pérez, R. Miranda, J. L. Carrascosa, P. A. Serena, M. de Ridder, A. Raman, J. Gómez-Herrero, I. A. T. Schaap, D. Reguera and P. J. de Pablo, *Biophys. J.*, 2011, **100**, 1100–1108.
21 A. Ortega-Esteban, A. J. Pérez-Berná, R. Menéndez-Conejero, S. J. Flint, C. San Martín and P. J. de Pablo, *Sci. Rep.*, 2013, **3**, 1434.
22 M. Hernando-Pérez, S. Lamber, E. Nakatani-Webster, C. E. Catalano and P. J. d. Pablo, *Nat. Commun.*, 2014, 5.
23 L. Fumagalli, D. Esteban-Ferrer, A. Cuervo, J. L. Carrascosa and G. Gomila, *Nat. Mater.*, 2012, **11**, 808–816.
24 R. H. French, V. A. Parsegian, R. Podgornik, R. F. Rajter, A. Jagota, J. Luo, D. Asthagiri, M. K. Chaudhury, Y. M. Chiang, S. Granick, S. Kalinin, M. Kardar, R. Kjellander, D. C. Langreth, J. Lewis, S. Lustig, D. Wesolowski, J. S. Wettlaufer, W. Y. Ching, M. Finnis, F. Houlihan, O. A. von Lilienfeld, C. J. van Oss and T. Zemb, *Rev. Mod. Phys.*, 2010, **82**, 1887–1944.
25 J. Israelachvili, *Intermolecular and surface forces*, Academic Press, London, 2011.
26 K. J. M. Bishop, C. E. Wilmer, S. Soh and B. A. Grzybowski, *Small*, 2009, **5**, 1600–1630.
27 T. Zemb and V. A. Parsegian, *Curr. Opin. Colloid Interface Sci.*, 2011, **16**, 515–516.
28 R. J. Nap, A. Lošdorfer Božič, I. Szleifer and R. Podgornik, *Biophys. J.*, 2014, **107**, 1970–1979.
29 S. Garcia-Manyes, G. Oncins and F. Sanz, *Biophys. J.*, 2005, **89**, 1812–1826.
30 J. Sotres and A. M. Baro, *Appl. Phys. Lett.*, 2008, **93**, 103903.
31 Y. F. Dufrene, D. Martinez-Martin, I. Medalsy, D. Alsteens and D. J. Muller, *Nat. Methods*, 2013, **10**, 847–854.
32 D. J. Müller, M. Amrein and A. Engel, *J. Struct. Biol.*, 1997, **119**, 172–188.
33 M. Radmacher, M. Fritz, C. Kacher and P. J. Cleveland, *Biophys. J.*, 1996, **70**, 556–567.
34 P. J. de Pablo, I. A. T. Schaap, F. C. MacKintosh and C. F. Schmidt, *Phys. Rev. Lett.*, 2003, **91**, 98101.
35 R. M. Pashley, *J. Colloid Interface Sci.*, 1981, **38**, 531–546.
36 V. A. Parsegian, *A Handbook for Biologists, Chemists, Engineers, and Physicists*, 2006.
37 A. Parsegian and D. Gingell, *Biophys. J.*, 1972, **12**, 1192–1972.
38 N. I. Abu-Lail and T. A. Camesano, *Biomacromolecules*, 2003, **4**, 1000–1012.

39 Y. Xiang, M. C. Morais, A. J. Battisti, S. Grimes, P. J. Jardine, D. L. Anderson and M. G. Rossmann, *EMBO J.*, 2006, **25**, 5229–5239.
40 M. C. Morais, S. Kanamaru, M. O. Badasso, J. S. Koti, B. A. L. Owen, C. T. McMurray, D. L. Anderson and M. G. Rossmann, *Nat. Struct. Biol.*, 2003, **10**, 572–576.
41 A. G. Cherstvy, *Phys. Chem. Chem. Phys.*, 2011, **13**, 9942–9968.
42 A. N. Giberson, A. R. Davidson and R. J. Parks, *Nucleic Acids Res.*, 2012, **40**, 2369–2376.
43 A. Ortega-Esteban, I. Horcas, M. Hernando-Pérez, P. Ares, A. J. Pérez-Berná, C. San Martín, J. L. Carrascosa, P. J. de Pablo and J. Gómez-Herrero, *Ultramicroscopy*, 2012, **114**, 56–61.
44 J. E. Sader, J. W. M. Chon and P. Mulvaney, *Rev. Sci. Instrum.*, 1999, **70**, 3967–3969.
45 I. Horcas, R. Fernandez, J. M. Gomez-Rodriguez, J. Colchero, J. Gomez-Herrero and A. M. Baro, *Rev. Sci. Instrum.*, 2007, 78.
46 B. W. Ninham and V. A. Parsegian, *J. Theor. Biol.*, 1971, **31**, 405–428.
47 S. Basak and A. Raman, *Appl. Phys. Lett.*, 2007, **91**, 1–3.
48 G. Lamm, *Rev. Comput. Chem.*, 2003, **19**, 147–365.
49 H. Ohshima and T. Kondo, *J. Colloid Interface Sci.*, 1993, **155**, 499–505.
50 J. E. Sader, S. L. Carnie and D. Y. C. Chan, *J. Colloid Interface Sci.*, 1995, **171**, 46–54.
51 A. Guasch, J. Pous, B. Ibarra, F. X. Gomis-Ruth, J. M. Valpuesta, N. Sousa, J. L. Carrascosa and M. Coll, *J. Mol. Biol.*, 2002, **315**, 663–676.
52 J. M. Valpuesta and J. L. Carrascosa, *Q. Rev. Biophys.*, 1994, **27**, 107–155.
53 W. R. Wikoff and J. E. Johnson, *Curr. Biol.*, 1999, **9**, R296–R300.
54 A. J. Pérez-Berná, R. Marabini, S. H. Scheres, R. Menéndez-Conejero, I. P. Dmitriev, D. T. Curiel, W. F. Mangel, S. J. Flint and C. San Martín, *J. Mol. Biol.*, 2009, **392**, 547–557.
55 E. F. Pettersen, T. D. Goddard, C. C. Huang, G. S. Couch, D. M. Greenblatt, E. C. Meng and T. E. Ferrin, *J. Comput. Chem.*, 2004, **25**, 1605–1612.

